h0472DNA Base Properties from *First Principles* Plane-Wave Calculations

Martin Preuß, Kaori Seino, and Wolf G. Schmidt

Computational Materials Science Group
Friedrich-Schiller-Universität
Max-Wien-Platz 1, 07743 Jena, Germany
preuss@ifto.physik.uni-jena.de

Abstract. We present equilibrium geometries, dipole moments, ionization energies and electron affinities of the DNA base molecules adenine, thymine, guanine, and cytosine calculated from *first principles*. The comparison of our results with experimental data and results obtained by using quantum chemistry methods shows that gradient-corrected density-functional theory (DFT-GGA) calculations using ultrasoft pseudopotentials and a plane-wave basis are a numerically efficient and accurate alternative to methods employing localized orbitals for the expansion of the electron wave functions.

1 Introduction

Quantum chemistry methods range from empirical molecular dynamics over density-functional theory (DFT) implementations with localized basis sets to wave-function based methods. The latter, e. g., Hartree-Fock, Møller-Plesset [1] or coupled-cluster methods [2,3], can be very accurate, but due to their unfavourable scaling properties are applicable only to a small number of atoms. In addition, if atom-centered functions form the basis set, calculations suffer from an inherent inaccuracy known as the basis set superposition error (BSSE). Controversies still exist with regard to the validity of counterpoise correction schemes [4] that are designed to correct for the BSSE (see, e.g., [5]). Moreover, the usage of a necessarily incomplete basis set such as Gaussians for the expansion of the molecular electron wave function renders the efficient and reliable control of the numerical convergence difficult. These problems do not exist if, instead, plane waves are used for the expansion of the wave functions. Furthermore, the implementation of periodic boundary conditions is straightforward, thus allowing for the treatment of extended systems. This is especially important when studying the interaction of molecules with crystals surfaces as planned for the further stages of our project. However, a serious

disadvantage of plane-wave based methods for the treatment of finite systems is the relatively high number of plane waves needed to obtain numerically converged results, especially if first-row elements of the periodic table such as carbon, nitrogen and oxygen are concerned. The numerical demand can in principle be drastically reduced by employing ultrasoft, non-normconserving pseudopotentials to describe the electron-ion interaction [6].

Therefore we probe here the applicability of DFT in the generalized gradient approximation (GGA) [7,8] together with ultrasoft pseudopotentials and a plane-wave basis set. We show that accurate and numerically converged molecular structures can be obtained already with a relatively low cutoff energy. The same approach is then applied to study the electronic properties of the DNA base molecules.

2 Computational Method

2.1 Kohn-Sham energy functional for ultrasoft pseudopotentials

The starting point for the total-energy calculations in conjunction with ultrasoft pseudopotentials (US PP) is the Kohn-Sham energy functional which can be written as [9,10]

$$E_{\mathrm{KS}}[\{\phi\},\{\mathbf{R}\}] = \sum_{n=1}^{N_b} f_n \langle\phi_n|\hat{T} + \hat{V}_{\mathrm{nl}}^{\mathrm{ion}}|\phi_n\rangle + E_{\mathrm{H}}[n] + E_{\mathrm{XC}}[n] + \int \mathrm{d}\mathbf{r}\, V_{\mathrm{loc}}^{\mathrm{ion}}(\mathbf{r}) n(\mathbf{r}) + \gamma_{\mathrm{Ewald}}(\{\mathbf{R}\}) \tag{1}$$

with $f_n = 1$ for occupied and $f_n = 0$ for unoccupied bands. To simplify notation the k-index has been dropped. The sum runs over the N_b bands included in the calculation. The functional E_{KS}, dependent only on the electronic wavefunctions ϕ_n and the atomic positions $\mathbf{R}$, is decomposed into the classical Hartree energy E_{H}, the local ionic pseudopotential $V_{\mathrm{loc}}^{\mathrm{ion}}$, the kinetic energy operator $\hat{T}$ with $T = -\hbar^2/2m\Delta$ and the Madelung energy γ_{Ewald} of the ions. The remaining matrix elements $\langle\phi_n|\hat{V}_{\mathrm{nl}}^{\mathrm{ion}}|\phi_n\rangle$ are derived from the nonlocal part of the pseudopotential which can be cast into the form

$$\hat{V}_{\mathrm{nl}}^{\mathrm{ion}} = \sum_{ij} D_{ij}^{\mathrm{ion}} |\beta_j\rangle\langle\beta_i| \tag{2}$$

with localized projection states $|\beta_i\rangle$. With the projection operators the overlap matrix is constructed,

$$\hat{S} = \hat{1} + \sum_{ij} q_{ij} |\beta_j\rangle\langle\beta_i| \,, \tag{3}$$

q_{ij} denoting the so-called augmentation charges. Thus the nonlocality of the ultrasoft pseudopotential gives rise to the generalized orthonormalization constraint

$$\langle \phi_m | \hat{S} | \phi_n \rangle = \delta_{mn}. \tag{4}$$

Minimizing the Kohn-Sham functional with respect to the wavefunctions and subject to the orthonormalization constraint leads to the modified Kohn-Sham equations

$$\hat{H} | \phi_n \rangle = \varepsilon_n \hat{S} | \phi_n \rangle \tag{5}$$

in the form of a *generalized* eigenvalue problem. This complication is counterbalanced by a reduction of the necessary cutoff for first-row elements by a factor between 2 and 4 compared to normconserving pseudopotentials for systems of the size studied here.

A major advantage of using plane waves as a basis for the expansion of the electron wave functions ϕ_n is the fact that the local part of the pseudopotential and the kinetic energy operator are diagonal in real and reciprocal space, respectively. Therefore the evaluation of the action of the Hamiltonian $\hat{H}$ is very fast when using the Fast Fourier Transform (FFT) to transform the wavefunctions to reciprocal space and back. Together with separable factorized pseudopotentials [11] these features allow for the application of highly efficient iterative diagonalization algorithms to solve the Kohn-Sham equations.

To this end we employ the *residual minimization method – direct inversion in the iterative subspace* (RMM-DIIS) algorithm [12,13] using the Vienna Ab-initio Simulation Package (VASP) implementation [14] of the gradient-corrected (PW91) [7] density functional theory together with highly transferable ultrasoft pseudopotentials [6] supplied with the code.

2.2 Computational cost

In the RMM-DIIS algorithm the calculation of the residual $(\hat{H} - \varepsilon \hat{S}) | \phi_n \rangle$ is an operation of the order $N^2 \log N$, N being the number of atoms. The most demanding parts in the calculation of the action of $\hat{H}$ and $\hat{S}$ are the FFT and the evaluation of the nonlocal projection operators. For larger systems they are calculated in real space [15] and therefore the number of operations per band increases linearly with the system size. For all bands this is only an $\mathcal{O}(N^2)$ operation. The orthogonalization of the wave functions and the subspace diagonalization scale like $\mathcal{O}(N^3)$ with similar prefactors that are small compared to those of the $\mathcal{O}(N^2)$ operations. Thus their contribution to the overall execution time becomes dominant only for systems containing more than about 10^3 atoms. This favourable scaling behaviourhas allowed for modeling semiconductor structures containing nearly 3000 atoms using VASP [16].

VASP offers parallelization over bands and plane-wave coefficients. To reduce communication overhead VASP uses a twodimensional cartesian topology in which the bands are distributed among a group of nodes in a round-robin fashion. Using MPI functionality, in-group communication does not interfere with inter-band communication. It should be noted that parallelization over plane-wave coefficients results in large memory demands because the

Table 1: Details of a ground-state calculation from scratch for the DNA base guanine on the Hitachi-SR8000.

number of atoms	16	number of bands	45
size of supercell	$10\times20\times20$ Å^3	max. number of plane waves	47190
number of nodes	32	integrated memory used	14409 MB
CPU time	1522 s	max. memory used per node	496 MB
MFlops	1914		

nonlocal projection operators $|\beta_j\rangle\langle\beta_i|$ must be stored on each node within a group. Table 1 summarizes the details of a typical ground-state calculation for guanine on the Hitachi-SR8000.

3 Results and Discussion

We performed extensive convergence tests on gas-phase adenine using a $10\times20\times20$ Å^3 supercell. The total energy and characteristic bond lengths are found to be completely converged (and the latter in excellent agreement with experiment, cf. Fig. 1) if the electronic wave functions are expanded into plane waves up to a kinetic energy of 35 Ry. This constitutes a major computational saving, compared to the cutoff energy of 70 Ry found necessary in calculations using norm-conserving pseudopotentials [17, 18]. For adenine, cytosine and guanine (thymine) the cutoff of 35 Ry corresponds to a basis set of roughly 45000 (94000) plane waves. This still relatively high number

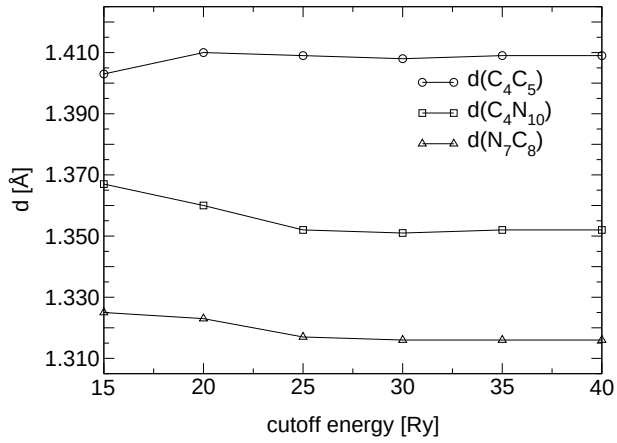

Fig. 1: Equilibrium bond lengths (cf. Fig. 2) of gas-phase adenine vs the plane-wave cutoff energy.

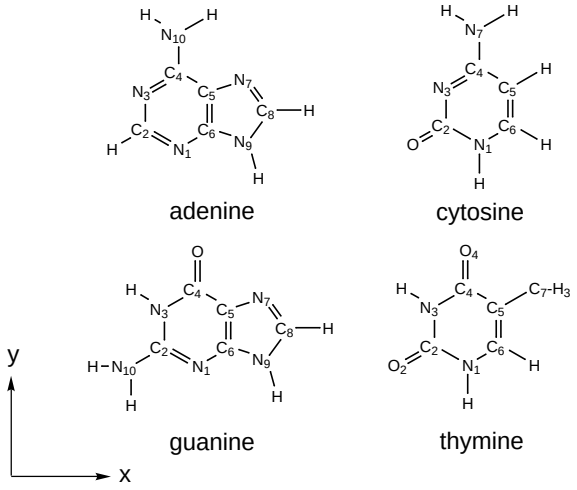

Fig. 2: Schematic structures of most stable tautomers of the DNA bases

results from the requirement to also 'describe' the large vacuum region of the supercell. Therefore the favorable scaling properties of the VASP implementation (compared to the scaling worse than $\mathcal{O}(N^4)$ for post-Hartree-Fock methods [19]) do not necessarily translate into a short execution time for systems such as studied here, cf. Table 1.

As can be seen from Fig. 1, the energy cutoff can be further reduced to 25 Ry, on the expense of a slightly increased error bar. We use the value of 35 Ry throughout the calculations. In the case of thymine the size of the supercell had to be increased to $20\times20\times20$ Å^3.

3.1 Geometries

Calculated bond lengths for the most stable tautomers of the DNA bases, i.e., the keto-forms shown in Fig. 2, are compiled in Tab. 3.1. They are compared with high-resolution X-ray and neutron diffraction data summarized in a statistical survey of the *Cambridge Structural Database* by Clowney *et al.*, see Ref. [20]. The standard deviations in the samples amount to less than 0.002 Å for the bond lengths. The calculated values and the cited experimental findings agree within an error bar of typically less than 1–2 %. A slight overestimation of bond lengths of this order of magnitude is to be expected for DFT-GGA calculations [21]. The bond lengths of DNA base molecules have also been determined using a variety of quantum chemical methods such as MP2/6-31G(d,p) [22, 23], HF/4-31G [24], and B3LYP/6-311G(d,p) calculations [25]. The comparison of these predictions (also given in Tab. 3.1) with the data presented here shows that plane-wave calculations using ultrasoft pseudopotentials are comparable in accuracy with those quantum-chemical

approaches concerning the bond lengths. Our results are also very close to those obtained in a recent DFT-GGA study using plane waves in conjunction with normconserving pseudopotentials [26].

Table 2: Calculated bond lengths (in Å) for adenine, cytosine, guanine, and thymine. Comparison is made with experimental data from Ref. [20] and quantum-chemical results from Refs. [22, 24, 25].

adenine				cytosine			
bond	DFT-GGA	Ref. [25]	Exp.	bond	DFT-GGA	Ref. [22]	Exp.
N_1C_2	1.341	1.333	1.331	N_1C_2	1.429	1.418	1.399
C_2N_3	1.348	1.342	1.339	C_2O	1.231	1.226	1.237
N_3C_4	1.350	1.342	1.351	C_2N_3	1.367	1.382	1.356
C_4N_{10}	1.352	1.353	1.335	N_3C_4	1.324	1.318	1.334
C_4C_5	1.409	1.409	1.406	C_4N_7	1.359	1.369	1.337
C_5C_6	1.396	1.396	1.383	C_4C_5	1.435	1.437	1.426
C_6N_1	1.339	1.336	1.344	C_5C_6	1.360	1.359	1.337
C_5N_7	1.383	1.385	1.388	C_6N_1	1.353	1.358	1.364
N_7C_8	1.316	1.308	1.311				
C_8N_9	1.381	1.380	1.373				
N_9C_6	1.381	1.377	1.374				
guanine				thymine			
bond	DFT-GGA	Ref. [22]	Exp.	bond	DFT-GGA	Ref. [24]	Exp.
N_1C_2	1.312	1.310	1.323	N_1C_2	1.389	1.366	1.376
C_2N_{10}	1.361	1.385	1.337	C_2O_2	1.227	1.218	1.220
C_2N_3	1.371	1.372	1.371	C_2N_3	1.383	1.368	1.373
N_3C_4	1.434	1.430	1.391	N_3C_4	1.406	1.384	1.382
C_4O	1.230	1.225	1.238	C_4O_4	1.233	1.218	1.228
C_4C_5	1.435	1.442	1.419	C_4C_5	1.459	1.461	1.445
C_5C_6	1.402	1.394	1.379	C_5C_6	1.354	1.329	1.339
C_6N_1	1.354	1.366	1.350	C_6N_1	1.376	1.380	1.378
C_5N_7	1.380	1.377	1.388	C_5C_7	1.495	1.498	1.496
N_7C_8	1.311	1.324	1.305				
C_8N_9	1.385	1.375	1.374				
N_9C_6	1.370	1.370	1.375				

In contrast to the bondlengths, the planarity of the nucleic acid bases is still under debate. For a detailed discussion see [27, 28]. Whereas earlier *ab initio* calculations carried out at the Hartree-Fock level indicate a rather weak amino group pyramidalization [29] more recent studies predict dihedral angles of 39.1° for guanine and 27.1° for cytosine [28]. Our DFT-GGA calculations, however, result in quite small deviations from planarity, cf. Table 3. For guanine we obtain a dihedral angle of only 2.3°. Interestingly, the DFT-

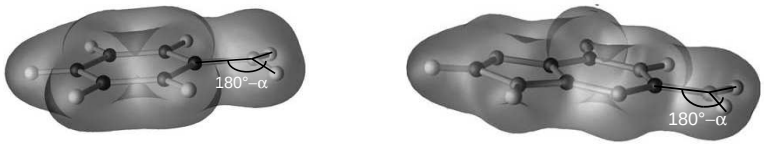

(a) aniline **(b)** guanine

Fig. 3: Electrostatic potential plotted on an isodensity surface for **(a)** aniline ($\alpha = 34.0°$) and **(b)** guanine ($\alpha = 2.3°$). The higher pyramidalization of the amino group in aniline leads to stronger charge accumulation at the nitrogen atom. For a reproduction of this figure in colour, see Fig. 35 on page 478.

GGA study by Di Felice et al. [26] on DNA bases also indicates a very weak nonplanarity.

The DFT-GGA approach thus seems not to be able to reproduce the order of amino group pyramidalization. But structural consequences of rehybridization processes at solid surfaces, which go along with strong charge inhomogeneities, are generally well accounted for in DFT calculations using LDA or GGA to model the effects of exchange and correlation [30, 31]. As, unfortunately, there are no experimental data available for the amount of nonplanarity of the DNA bases we performed additional calculations for aniline ($C_6H_5NH_2$). In this case we predict an out-of-plane angle of the amino group with respect to the ring plane of 34.0°, close to the experimental value of 37.5° obtained by microwave spectroscopy [32], cf. Fig. 3. For aniline, the HF/6-31G calculations in [28] yield a dihedral angle of 46.2°, largely overestimating the experiment.

Table 3: Nonplanarity of the DNA bases with amino-group

		rms deviation from planarity	
base	dihedral angle	C – NH_2-group	molecule
adenine	0.0°	0.000 Å	0.000 Å
cytosine	11.2°	0.028 Å	0.020 Å
guanine	2.3°	0.006 Å	0.023 Å

3.2 Dipole moments

The electronic properties of the DNA base molecules are less well understood than their structural details. The electrostatic potential around DNA bases is

Table 4: Calculated dipole moments in the three cartesian directions and absolute values (in Debye) of adenine (A), cytosine (C), guanine (G) and thymine (T).

	DFT-GGA				Exp.
	μ_x	μ_y	μ_z	μ	μ
A	−2.55	−0.29	0.00	2.56	2.5[a]
C	−5.51	−3.43	0.22	6.49	7.0[b]
G	5.33	−4.37	0.16	6.89	7.1[a]
T	0.53	−4.45	0.02	4.48	4.1[c]

[a] from Ref. [33] [b] from Ref. [34] [c] from Ref. [35]

of primary importance for molecular interactions like H-bonding, hydration, and the bonding of small or polyvalent cations. The calculated dipole values of the DNA bases are compiled in Table 4; their components perpendicular to the molecular planes are almost neglegible because of their near planarity.

The comparison to experiment shows that electronic ground state properties, at least concerning the dipole moments, are reliably described within DFT-GGA. The agreement in the case of adenine is excellent while for thymine the dipole moment is slightly overestimated. The calculated values for cytosine and guanine are smaller than measured but are, however, very close to the results of quantum chemical calculations. The MP2/aug-cc-pVDZ values by Hobza and Šponer [27], for example, amount to 2.56, 6.49, 6.65, and 4.37 Debye for adenine, cytosine, guanine, and thymine, respectively. Similar values are also reported in [36].

3.3 Ionization energies and electron affinities

The calculation of excited configurations within DFT is a priori complicated because density-functional theory, by derivation, only describes the electronic ground state correctly. There exist well-founded schemes based on DFT plane-wave implementations that allow for a systematic improvement of the description of the electronic many-body effects in the excited states. This concerns both the inclusion of electronic self-energy effects for the accurate description of unoccupied electronic states within the GW method [37–39] and the Bethe-Salpeter equation (BSE) for pair excitations in order to account for electron-hole attraction contributions to the optical response [40–44]. In contrast to time-dependent density-functional theory (TDDFT), GW and BSE based approaches yield reliable results for both localized and extended systems [45,46]. These approaches are, however, computationally extremely expensive. In the present case the localization of the electronic states fortunately allows for a numerically far less demanding treatment of these many-body effects: we investigate their influence by means of delta self-consistent field (ΔSCF) – also called constrained-DFT – calculations. Thereby the total-energy differences between the ground states and the excited states of the molecules are

calculated. The electrons are allowed to relax, while the occupation numbers are constrained to the excited configuration. Here we determine the lowest single-electron excitation, the ionization energy (IE)

$$\mathrm{IE} = E(N-1) - E(N), \tag{6}$$

and the electron affinity (EA)

$$\mathrm{EA} = E(N) - E(N+1), \tag{7}$$

where $E(N)$ denotes the ground-state energy of the molecule with N electrons. The ionized molecules with one missing or additional electron are characterized by the total energies $E(N-1)$ and $E(N+1)$, respectively. Using (6) and (7), the calculation of single-particle excitation energies reduces to the treatment of electronic ground states. In addition, structural relaxations can be

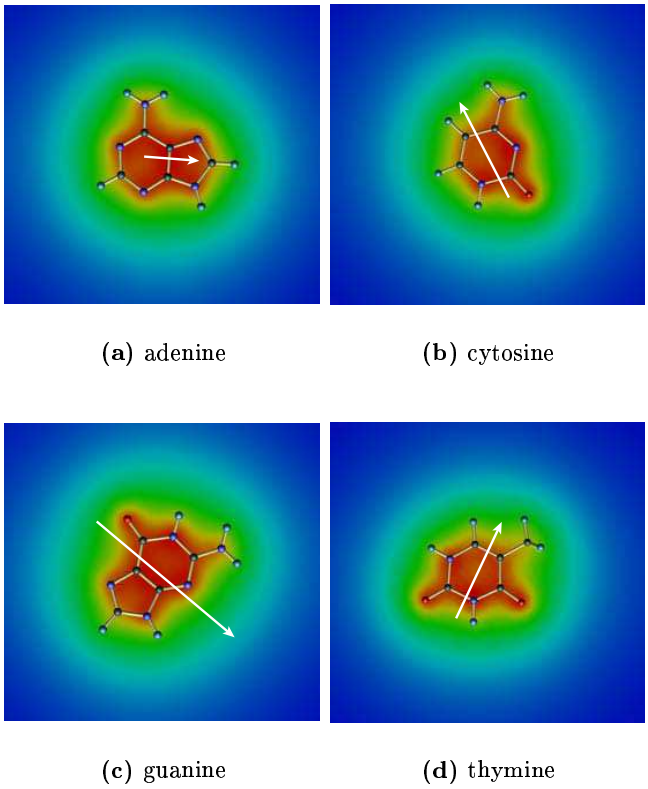

(a) adenine **(b)** cytosine

(c) guanine **(d)** thymine

Fig. 4: Hartree potential of the DNA bases in the molecular planes. The magnitudes and directions of the electric dipole moments are indicated by arrows. For a reproduction of this figure in colour, see Fig. 36 on page 478.

Table 5: Calculated ionization energies and electron affinities (in eV) of adenine (A), cytosine (C), guanine (G) and thymine (T).

	ionization energies		electron affinities	
	vertical	adiab.	vertical	adiab.
A	8.23	8.06	0.74	0.79
C	8.75	8.66	0.84	0.84
G	7.82	7.63	0.84	0.85
T	9.13	9.08		

taken into account. Then, instead of the vertical IEs and EAs, which include only electronic relaxation effects, one obtains adiabatic values.

The vertical and adiabatic values of the IEs and EAs computed within the ΔSCF schemes (6) and (7) are listed in Table 5. The effect of structural relaxation on the IEs amounts to about 0.1–0.2 eV. In contrast, this effect is negligible for the EAs. The additional electron in the LUMO state does not induce a noticeable change of the atomic geometry compared to the ground state.

Experimentally, adiabatic IEs of 8.26, 8.68, 7.77 and 8.87 eV were determined for adenine, cytosine, guanine, and thymine [47]. These values agree within 0.2 eV with our calculations. An error bar of the same size has been found in earlier quantum chemistry calculations [48]. The comparison of the calculated vertical IEs with the experimental results of 8.44, 8.94, 8.24, and 9.14 eV for adenine, cytosine, guanine, and thymine [49] is of the same accuracy. Only the agreement for guanine is worse. There is quite a scatter in the theoretical values, ranging for guanine for example from 7.31 eV determined with ΔSCF B3LYP/6-31G* calculations [50] to 8.1 eV obtained using a semi-empirical NDDO-G approach [51].

Because we did not obtain fully converged results for thymine, EAs calculated within the ΔSCF method are only cited for adenin, cytosine, and guanine. A delocalized excess electron presents an obvious obstacle to an accurate ΔSCF calculation of the EA within the supercell approach. In order to illustrate the degree of delocalization, we plot in Fig. 5 the orbital character of the adenine LUMO after one electron has been added. Upon electron addition and subsequent relaxation of the LUMO the orbital is partially smeared out in a region more than 5 Å away from the molecule. It extends over a large fraction of the supercell. Due to the periodic boundary conditions it is necessarily influenced by the neighboring images. Consequently, the electronic relaxation is not modeled correctly and the supercell ΔSCF calculation fails to account for the measured EA.

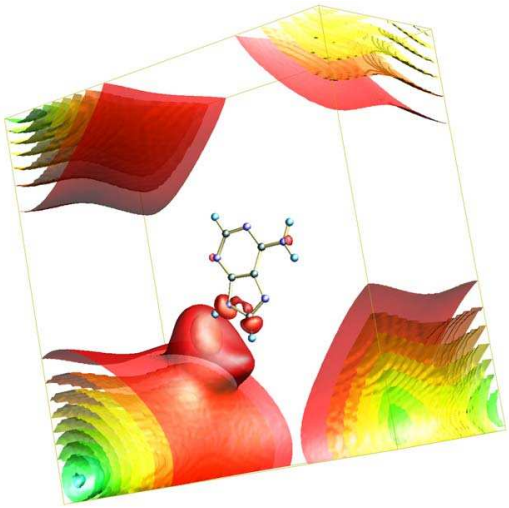

Fig. 5: Delocalized additional electron in the adenine LUMO. Edges of the supercell are indicated. For a reproduction of this figure in colour, see Fig. 37 on page 479.

4 Summary

We have been able to reproduce the molecular structures of the nucleic acid bases with the help of density-functional theory in conjuction with a plane-wave basis set and ultrasoft pseudopotentials. Concerning geometries, this method is comparable in accuracy to quantum-chemical approaches employing localized basis sets. We have applied our numerically converged *ab initio* method to examine the electronic properties of the DNA bases for which only little and/or contradicting information is available. Our results suggest the application of the VASP code also for further planned studies on the self-organization of DNA bases on solid surfaces.

Acknowledgement. Generous grants of computer time from the Leibniz-Rechenzentrum München are gratefully acknowledged.

References

1. C. Møller and M. S. Plesset, Phys. Rev. **46**, 618 (1934).
2. K. Raghavachari, G. W. Trucks, J. A. Pople, M. Head-Gordon, Chem. Phys. Lett. **157**, 479 (1989).
3. J. D. Watts, J. Gauss, R. J. Bartlett, J. Chem. Phys. **98**, 8718 (1993).
4. S. F. Boys and F. Bernardi, Mol. Phys. **19**, 553 (1970).
5. A. Hamza, A. Vibok, G. J. Halasz, I. Mayer, J. Mol. Struc. - Theochem **501**, 427 (2000).

6. J. Furthmüller, P. Käckell, F. Bechstedt, G. Kresse, Phys. Rev. B **61**, 4576 (2000).
7. J. P. Perdew, J. A. Chevary, S. H. Vosko, K. A. Jackson, M. R. Pederson, D. J. Singh, C. Fiolhais, Phys. Rev. B **46**, 6671 (1992).
8. J. P. Perdew, K. Burke, M. Enzerhof, Phys. Rev. Lett. **77**, 3865 (1996).
9. D. Vanderbilt, Phys. Rev. B **41**, 7892 (1990).
10. K. Laasonen, A. Pasquarello, R. Car, C. Lee, D. Vanderbilt, Phys. Rev. B **47**, 10142 (1992).
11. L. Kleinman and D. M. Bylander, Phys. Rev. Lett. **48**, 1425 (1982).
12. P. Pulay, Chem. Phys. Lett. **73**, 393 (1980).
13. D. M. Wood and A. Zunger, J. Phys. A **18**, 1343 (1985).
14. G. Kresse and J. Furthmüller, Comp. Mat. Sci. **6**, 15 (1996).
15. R. D. King-Smith, M. C. Payne, J. S. Lin, Phys. Rev. B **44**, 13063 (1991).
16. L. E. Ramos, J. Furthmüller, F. Bechstedt, L. M. R. Scolfaro, J. R. Leite, Phys. Rev. B **66**, 075209 (2002).
17. R. S. Fellers, D. Barsky, F. Gygi, M. Colvin, Chem. Phys. Lett. **312**, 548 (1999).
18. F. L. Gervasio, P. Carloni, M. Parrinello, Phys. Rev. Lett. **89**, 108102 (2002).
19. W. Kohn, Rev. Mod. Phys. **71**, 1253 (1999).
20. L. Clowney, S. C. Jain, A. R. Srinivasan, J. Westbrook, W. K. Olson, H. M. Berman, J. Am. Chem. Soc. **118**, 509 (1996).
21. M. Fuchs and M. Scheffler, Phys. Rev. B **57**, 2134 (1998).
22. Y. Podolyan, Y. V. Rubin, J. Leszczynski, J. Phys. Chem. A **104**, 9964 (2000).
23. J. Šponer and P. Hobza, J. Phys. Chem. **98**, 3161 (1994).
24. M. K. Shukla and P. C. Mishra, Chem. Phys. **240**, 319 (1999).
25. J. D. Gu and J. Leszczynski, J. Phys. Chem. A **103**, 2744 (1999).
26. R. Di Felice, A. Calzolari, E. Molinari, A. Garbesi, Phys. Rev. B **65**, 045104 (2001).
27. P. Hobza and J. Šponer, Chem. Rev. **99**, 3247 (1999).
28. J. Šponer and P. Hobza, Int. J. Quant. Chem. **57**, 959 (1996).
29. J. Leszynski, Int. J. Quantum Chem. **43**, 19 (1992).
30. C. Kress, M. Fiedler, W. G. Schmidt, F. Bechstedt, Phys. Rev. B **50**, 17697 (1994).
31. F. Bechstedt, A. A. Stekolnikov, J. Furthmüller, P. Käckell, Phys. Rev. Lett. **87**, 016103 (2001).
32. D. G. Lister, J. K. Tyler, J. H. Høg, N. W. Larsen, J. Mol. Struct. **23**, 253 (1974).
33. H. DeVoe and I. Tinoco, Jr, J. Mol. Biol. **4**, 500 (1962).
34. H.-P. Weber and B. M. Craven, Acta Crystallogr. **B46**, 532 (1990).
35. I. Kulakowski, M. Geller, B. Lesyng, K. L. Wierzcho, Biochim. Biophys. Acta **361**, 119 (1974).
36. J. B. Li, J. H. Xing, C. J. Cramer, D. G. Truhlar, J. Chem. Phys. **111**, 885 (1999).
37. F. Bechstedt, in: U. Rössler, ed., *Festkörperprobleme/Advances in Solid State Physics*, vol. 32, p. 161, Vieweg, Braunschweig/Wiesbaden (1992).
38. F. Aryasetiawan and O. Gunnarsson, Rep. Prog. Phys. **61**, 237 (1998).
39. W. G. Aulbur, L. Jonsson, J. W. Wilkins, *Solid State Physics: Advances in Research and Applications*, vol. 54, chap. Quasiparticle calculations in solids, p. 1, Academic, San Diego (2000).
40. S. Albrecht, L. Reining, R. Del Sole, G. Onida, Phys. Rev. Lett. **80**, 4510 (1998).

41. L. X. Benedict, E. L. Shirley, R. B. Bohn, Phys. Rev. Lett. **80**, 4514 (1998).
42. M. Rohlfing and S. G. Louie, Phys. Rev. Lett. **81**, 2312 (1998).
43. P. H. Hahn, W. G. Schmidt, F. Bechstedt, Phys. Rev. Lett. **88**, 016402 (2002).
44. W. G. Schmidt, S. Glutsch, P. H. Hahn, F. Bechstedt, Phys. Rev. B **67**, 085307 (2003).
45. I. Vasiliev, S. Ögüt, J. R. Chelikowsky, Phys. Rev. B **81**, 4959 (1999).
46. G. Onida, L. Reining, A. Rubio, Rev. Mod. Phys. **74**, 601 (2002).
47. V. M. Orlov, A. N. Smirnov, Y. M. Varshavsky, Tetrahedron Lett. **48**, 4377 (1976).
48. N. Russo, M. Toscano, A. Grand, J. Comput. Chem. **21**, 1243 (2000).
49. N. S. Hush and A. S. Cheung, Chem. Phys. Lett. **34**, 11 (1975).
50. F. Prat, K. N. Houk, C. S. Foote, J. Am. Chem. Soc. **120**, 845 (1998).
51. A. A. Voityuk, J. Jortner, M. Bixon, N. Rösch, Chem. Phys. Lett. **324**, 430 (2000).